A Numerical Analysis of the Bearing Vibration Response under Varying Outer Race Defect Positions

Thabisang Sylvester Lekalakala
Department of Industrial Engineering, Operations Management and Mechanical Engineering, Vaal University of Technology, Vanderbijlpark, South Africa
213076446@edu.vut.ac.za (corresponding author)

Alfayo Anyika Alugongo
Department of Industrial Engineering, Operations Management and Mechanical Engineering, Vaal University of Technology, Vanderbijlpark, South Africa
alfayoa@vut.ac.za

Bernard Xavier Tchomeni
Department of Industrial Engineering, Operations Management and Mechanical Engineering, Vaal University of Technology, Vanderbijlpark, South Africa
bernardt@vut.ac.za

Desejo Filipeson Sozinando
Department of Industrial Engineering, Operations Management and Mechanical Engineering, Vaal University of Technology, Vanderbijlpark, South Africa
desejos@vut.ac.za

Received: 20 August 2025 | Revised: 17 September 2025 | Accepted: 27 September 2025

 DOI: https://doi.org/10.48084/etasr.14210

ABSTRACT

A dynamic model of a ball bearing with an outer race spall defect was formulated to investigate the influence of the defect angular position on the vibration response. The model integrates Hertzian contact deformation, elastic energy principles, and a mathematical representation of the spall geometry within the bearing system. The governing equations of motion were derived using the Lagrangian approach and solved numerically through a fourth-order Runge–Kutta method. Defect orientations at 0°, 90°, 180°, and 270° were examined to capture the variations in system behavior. The time-domain analysis revealed periodic impact signals corresponding to the successive rolling elements striking the defect. The most severe vibratory amplitudes occurred at 270°, where the defect coincides with the zone of maximum radial load. In contrast, positions away from this load zone exhibited weaker responses due to the reduced contact forces. The envelope analysis highlighted modulation at the Ball Pass Frequency of the Outer Race (BPFO) and its higher harmonics, confirming the diagnostic significance of defect-induced excitations. The results demonstrated that defect orientation plays a crucial role in shaping vibration signatures, and accurate fault detection depends on accounting for angular position effects in the condition monitoring of rotating machinery.

Keywords-ball-bearing; Hertzian contact; outer race spall defect; envelope analysis; time-domain analysis

I. INTRODUCTION

Bearings are machine elements aiming to constrain motion in the desired direction and to reduce friction between moving parts while carrying loads. A variety of faults can develop in bearing systems, reducing performance and potentially causing premature failure of other machine components. Such faults include, but are not limited to, spalling, cracks, and pits [1]. Authors in [2] stated that spalling is commonly attributed to uncontrolled loading, unrestrained preload, tightly fitted inner rings, and prolonged operation beyond their specified fatigue life. Misalignment has also been widely studied, with findings showing that the higher degree of misalignment leads to elevated operating temperatures and concentrated Hertzian

stresses on the outer race surfaces [3]. Authors in [4] extended the diagnostic method to inner race cracks, broadening the scope of bearing fault detection.

Among these defects, outer race spall defects are particularly significant because they induce distinct vibration signatures that can be analyzed for diagnostic purposes [5]. Advancements have focused on integrating deformation characteristics into dynamic models to enhance the accuracy of fault detection and analysis. For instance, a new impact model for defective ball bearings considers defect width, depth, and ball-raceway contact deformations, factors that were previously overlooked, to simulate actual vibration signals more accurately [6]. Similarly, the quasi-static model based on the Jones-Harris model and Hertz contact theory highlights the importance of centrifugal force and structural parameters, such as the number of balls and groove curvature, in influencing the dynamic properties and fatigue life of bearings [7]. Additionally, the mechanical analysis of angular contact ball bearings revealed that rotor deformation significantly affects the support force and load distribution. The moment load on bearings increases with rotor length and hollowness [8]. The outer race defects and their impact on vibration characteristics under unbalanced conditions have also been modeled using the Hertzian contact deformation theory to emphasize the role of defect geometry and radial clearance [9]. Finally, innovative solving methods for bearing dynamics models, such as using contact angles as iterative variables, have improved the accuracy and efficiency of simulations. This approach highlights the influence of contact angles on bearing fatigue life [10]. Dynamic models have been further refined to include defect deformation and instantaneous impact force excitation, providing a more precise representation of the fault mechanisms in deep groove ball bearings [11]. Outer race defects in bearings are known to generate characteristic vibration signatures due to repeated impacts as the rolling elements strike the damaged area. Authors in [12] demonstrated that the defect's angular position significantly influences the amplitude and phase of the generated impulses.

For instance, experimental work on defects at 0°, 45°, and 180° revealed that when the defect was placed directly under the radial load zone, the resulting signals exhibited the highest RMS values [13]. Similarly, authors in [14] investigated the defect orientations at 0°, 45°, 90°, 135°, and 180°, and primarily assessed the effect of orientation through RMS variations. Authors in [15] also employed RMS as a statistical parameter within an ABAQUS finite element framework to evaluate orientation effects.

The above studies established the influence of outer race defect orientation on vibration signatures. However, their analyses were mostly confined to the loaded region of the bearing, which does not fully reflect real operating conditions, where a defect may occur anywhere along the outer race circumference. Moreover, orientation effects have been studied using statistical parameters, such as RMS, which, while simple, provide no frequency information and cannot distinguish between fault types, since outer race, inner race, and rolling element defects may all produce similar RMS changes. Therefore, it is important to extend orientation analysis by systematically covering the principal defect positions to ensure a comprehensive circumferential representation of the outer race, and to complement time-domain analysis with envelope spectrum analysis. While time-domain analysis is valuable for characterizing the dynamic response of the ball-raceway system, envelope spectrum analysis isolates defect-related frequency components, revealing distinct peaks at characteristic fault frequencies and their harmonics [16]. This combined approach enables a greater understanding of the bearing dynamics and enhances the diagnostic reliability.

The present study developed a dynamic model that integrates the Hertzian contact theory, spall defect representation, and energy-based principles. The model was utilized to evaluate the influence of outer race defect orientation on vibration characteristics in time-domain and envelope spectrum analyses.

II. BALL BEARING MODEL

The ball bearing model includes the outer race, inner race, rolling elements, cage, and an outer race defect. The elastic deformation theory was utilized to model the contact forces between the rolling elements and races, and the viscous fluid theory to account for damping due to lubricant films. The model also considers the radial motion of the balls around the bearing, where each ball dynamically contacts both races as it rotates. Contact interactions are represented by nonlinear springs in series, modeling the elastic interfaces between the ball and races, based on Hertzian contact theory. The damping effects are modeled by viscous dampers, also arranged in series. In combination, this spring-damper system captures the mechanical and fluid dynamics of the bearing under operation.

The following assumptions were considered in the model:

- Motion is permitted in the plane of the bearing only: axial motion is neglected.
- The model assumes a pure rolling contact between the balls and raceways, and therefore neglects ball slippage.
- The model incorporates a static radial preload applied through the stiffness terms K_s and K_{out}.
- The bearing operates under isothermal conditions.
- Contact and deformation occur according to the Hertzian elastic theory.
- The bearing rings have no global deformation: only local deformation is considered due to contact stresses.
- The contact damping force is considered according to the viscous fluid theory.

Figure 1 illustrates the 2D ball bearing dynamic model comprising a shaft-inner race assembly modeled as M_{in}. Its motion is permitted in x and y translations and in rotation. (θ_{in}). The assembly undergoes global stiffness and damping, represented by K_s and C_s, respectively. The rolling elements, modeled as m_b, have rotational motion about their centers (θ_b) and radial motion as they orbit the bearing center. The contacts between the rolling elements and raceways are modeled as Hertzian contact springs (K_{in} and K_{out}), while the lubrication

effects are represented by a damper c_b. The outer race is stationary and rigidly fixed to a non-deformable housing.

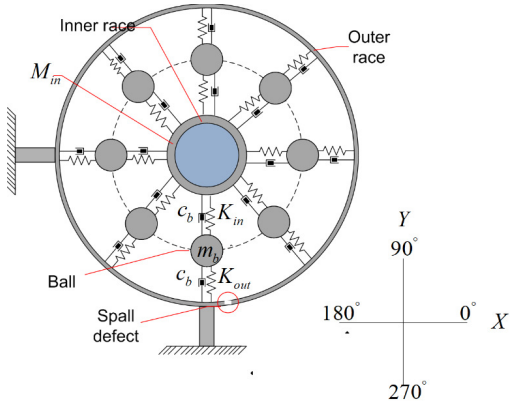

Fig. 1. Ball bearing model containing rolling elements, inner race, outer race, and spall defect.

III. SYSTEM ENERGIES

The shaft and inner race are rigidly fixed, meaning that they rotate and vibrate as a single unit. Their kinetic energy emanates from two types of motions: rotational and translational. Similarly, the rolling elements are considered rigid bodies. Figure 2 shows that their kinetic energy is derived from both their translational and rotational motion as they orbit the bearing center.

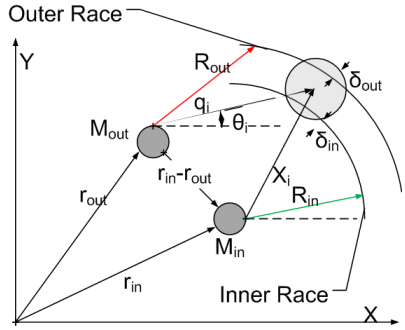

Fig. 2. The relative movement of bearing components and the deflection of the i-th ball.

The total kinetic energy of the system is thus expressed as:

$$T_{total} = \frac{1}{2}M_{in}\dot{x}_{in}^{\ 2} + \frac{1}{2}M_{in}\dot{y}_{in}^{\ 2} + \frac{1}{2}J_{in}\dot{\theta}_{in}^{\ 2} + \sum_{i=1}^{z}\frac{1}{2}m_b\left(q_i^{\ 2}\dot{\theta}_i^{\ 2} + \dot{q}_i^{\ 2}\right) + \frac{1}{2}J_b\dot{\theta}_i^{\ 2}\left(1+\frac{R_{out}}{R_b}\right)^2 \quad (1)$$

The potential energy of the system is modeled on two primary sources of stiffness: the contact stiffness at the rolling element-raceway interfaces, as depicted in Figure 2, and the translation stiffness associated with lateral displacement of the shaft-inner race assembly. These stiffness components have a significant influence on the system's potential energy and are expressed as:

$$U_T = \frac{1}{2}K_s x_{in}^2 + \frac{1}{2}K_s y_{in}^2 + \sum_{i=1}^{z}\frac{1}{2}K_{in}\delta_{in}^2 + \sum_{i=1}^{z}\frac{1}{2}K_{out}\delta_{out}^2 \quad (2)$$

As shown in Figure 2, the angular position of the i-th rolling element with respect to the outer race center is denoted by θ_i. The variable q_i defines the radial position vector from the center of the i-th rolling element relative to the outer race center, while X_i is the distance between the centers of the i-th element and the inner race.

The local deformation refers to the microscopic compression that occurs at the exact contact point between the rolling elements and the raceways (inner and outer). This is expressed as:

$$\delta_{in} = \left(R_{in} + R_b + C_r\right) - X_i \quad (3)$$

$$\delta_{out} = R_{out} - \left(R_b + q_i + C_r\right) \quad (4)$$

where R_{in}, R_{out}, R_b, and C_r represent the radii of the inner race, outer race, rolling elements (balls), and the radial clearance, respectively.

The Rayleigh dissipation function of the system arises from losses caused by damping forces. This damping is predominantly caused by viscous shear in the lubricant films, internal material friction (hysteresis) in the shaft, and interface damping at support connections. It is expressed as:

$$F_T = \frac{1}{2}C_s\dot{x}_{in}^2 + \frac{1}{2}C_s\dot{y}_{in}^2 + \sum_{i=1}^{z}\left[\left(\frac{1}{2}c_b\dot{\delta}_{in}^2\right) + \left(\frac{1}{2}c_b\dot{\delta}_{out}^2\right)\right] \quad (5)$$

The total dissipation function includes both the shaft damping and the contact damping due to the lubricant film.

IV. OUTER RACE SPALL DEFECT

Figure 3 displays the instant when the rolling element enters the defect region, marked by the point P_s, where the raceway curvature transitions from concave to convex. Beyond the inflection point, the rolling element begins to sink into the defect.

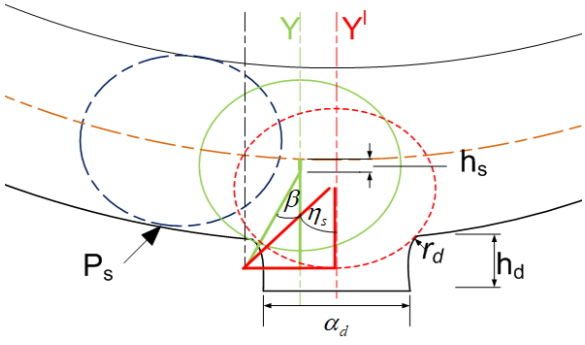

Fig. 3. Entry point of a rolling element into the defect.

When the rolling element (ball) has reached its maximum sink depth (red circle), the maximum angular span, η_s, is defined as:

$$\sin\eta_s = \frac{\left(\frac{a_d}{2} + r_d\right)}{\left(R_b + r_d\right)} \quad (6)$$

The sinking depth, h_s, is time varying: it increases progressively as the ball advances through the defect (green circle), reaching its maximum at the defect center. Thereafter, h_s decreases symmetrically until it returns to zero at the trailing edge, when the ball exits the defect region. This time-varying sink depth governs the overall contact deformation, directly influencing the corresponding forces in the system, and is expressed as:

$$h_s = \left(1 - \cos\beta\right)\left(R_b + r_d\right) \quad (7)$$

where R_b and r_d are the ball radius and defect edge radius, respectively. The local angle between the ball center and the contact point is expressed as:

$$\sin\beta = \frac{R_{outer} + r_d}{R_b + r_d}\sin\theta_i \quad (8)$$

where R_{outer} is the radius of the outer race.

V. SYSTEM EQUATIONS OF MOTION

The system energies, combined with the spall defect, are further derived using the Lagrangian approach to determine the equations of motion. This results in a three-degree-of-freedom (DOFs) system, described as:

$$\frac{d}{dt}\left(\frac{\partial T}{\partial \dot{g}_i}\right) - \frac{\partial T}{\partial g_i} + \frac{\partial F_c}{\partial \dot{g}_i} + \frac{\partial U}{\partial g_i} = Q_i \quad g_i = x_{in}, y_{in}, q_i \quad (9)$$

Considering the first generalized coordinate x_{in}:

$$M_{in}\ddot{x}_{in} + C_s\dot{x}_{in} + K_s x_{in} - \sum_{i=1}^{Z} K_{in}\left[\left(R_{in} + R_b + C_r + h_s\right) - X_i\right]\frac{\partial X_i}{\partial x_{in}} = 0 \quad (10)$$

Considering the second generalized coordinate y_{in}:

$$M_{in}\ddot{y}_{in} + C_s\dot{y}_{in} + K_s y_{in} - \sum_{i=1}^{Z} K_{in}\left[\left(R_{in} + R_b + C_r + h_s\right) - X_i\right]\frac{\partial X_i}{\partial y_{in}} = W \quad (11)$$

Considering the third generalized coordinate q_{in}:

$$m_b\ddot{q}_i - m_b q_i\dot{\theta}_i^2 + F_{q_i} = 0 \quad (12)$$

Where:

$$F_{q_i} = -K_{in}\left[\left(R_{in} + R_b + C_r + h_s\right) - X_i\right]\frac{\partial X_i}{\partial q_i} - K_{out}\left[R_{out} - \left(R_b + q_i + C_r + h_s\right)\right] + c_b\dot{X}_i\frac{\partial \dot{X}_i}{\partial \dot{q}_i} + c_b\dot{q}_i \quad (13)$$

$$X_i = \left(x_{in}^2 + q_i^2 - 2q_i x_{in}\cos\theta_i - 2q_i y_{in}\sin\theta_i + y_{in}^2\right)^{0.5} \quad (14)$$

$$\frac{\partial X_i}{\partial x_{in}} = \frac{-x_{in} - q_i\cos\theta_i}{X_i} \quad (15)$$

$$\frac{\partial X_i}{\partial y_{in}} = \frac{-y_{in} - q_i\cos\theta_i}{X_i} \quad (16)$$

$$\frac{\partial X_i}{\partial q_i} = \frac{\partial \dot{X}i}{\partial \dot{q}_i} = \frac{q_i - x_{in}\cos\theta_i - y_{in}\sin\theta_i}{X_i} \quad (17)$$

$$\dot{X}_i = \frac{1}{X_i}\left\{\begin{matrix} q_i\dot{q}_i + \dot{q}_{in}\left[-x_{in}\cos\theta_i - y_{in}\sin\theta_i\right] \\ +q_i\dot{\theta}_i\left[x_{in}\sin\theta_i - y_{in}\cos\theta_i\right] \end{matrix}\right\} \quad (18)$$

The presented equations of motion have been derived using the Lagrangian method. This method is particularly advantageous for modeling complex systems because it provides a systematic, energy-based framework that simplifies the derivation of complex nonlinear systems. By employing generalized coordinates, the model can effectively account for phenomena, such as contact deformation and damping, without the need to explicitly resolve all individual forces and reactions. In summary, the equations of motion provide a comprehensive dynamic representation of the ball bearing system, incorporating translational DOFs of the shaft-inner race and the radial deformation of the rolling elements.

VI. NUMERICAL TIME-DOMAIN SIMULATION AND ENVELOPE ANALYSIS OF THE BEARING SYSTEM

The dynamic response signal is obtained by solving the system's equations of motion using MATLAB's ODE solver, which is based on the 4th-order Runge-Kutta method. Initial conditions are applied to all 3 DOFs, and the resulting acceleration signal is recorded over time. To isolate the fault-related frequency components, the band-pass Butterworth filter is applied to the signal, eliminating unwanted low and high frequency noise. Subsequently, envelope analysis is performed to demodulate the signal and extract useful periodic impulses associated with bearing defects. The parameters of the simulated bearing are shown in Table I.

This approach enables the identification of characteristic defect frequencies, such as BPFO, even when the signal is masked by noise. The envelope spectrum, therefore, improves the reliability of defect diagnosis compared to the conventional Fourier transform-based methods.

Figure 4 illustrates the time-domain response of a ball bearing with an outer race defect positioned at various angular positions (0°, 90°, 180°, and 270°). The waveform exhibits a series of periodic impacts, corresponding to consecutive rolling elements striking the defect area as the bearing rotates. The periodic impacts are consistent with the results in [17], where it was demonstrated that outer race defects cause periodic impacts on the time-domain plot.

TABLE I. MODEL PARAMETERS FOR THE 6205 DEEP GROOVE BALL BEARING

Parameters of the simulated bearing	**Value**
Mass of the ball (m_b)	0.008 kg
Inner ring mass (M_{in})	0.15 kg
Inner raceway radius (R_{in})	12.5 mm
Outer raceway radius (R_{out})	26 mm
Bearing pitch diameter (P_d)	38.5 mm
Ball radius (R_b)	3.915 mm
Number of balls (z)	9
Radial clearance (C_r)	50 µm
Damping coefficient of balls due to fluid film (c_b)	1 × Ns/m
Inner race/ball stiffness (K_{in})	1×10^4 N/m
Outer race/ball stiffness (K_{out})	1×10^4 N/m
Stiffness of support shaft (K_s)	10×10^4 N/m
Shaft/inner race damping coefficient (C_s)	1 × Ns/m
Defect trailing edge radius (r_d)	0.0005 m
Defect length (a_d)	0.004 m
Defect depth (h_d)	0.0004 m

These impacts appear as bursts of acceleration with peak amplitudes of approximately ±1.25 mm/s^2, ±1 mm/s^2, ±0.4 mm/s^2, and ±5.2 mm/s^2 for 0°, 90°, 180°, and 270°, respectively. The regularity of the impacts aligns with the BPFO, confirming that the defect is consistently excited with each ball revolution. As shown in Figure 4(b), when the defect is positioned at 90° (top of the bearing), the rolling elements experience a minimal contact force due to the direction of the radial load. This reduced interaction lowers the peak amplitudes in the vibration response. This effect is also observed in Figure 4(a) and Figure 4(c) at the 0° and 180° defect positions, respectively. The most severe dynamic behavior occurs at 270° (bottom of the bearing), where the defect is fully aligned with the static radial load vector, as portrayed in Figure 4(d). This alignment leads to the highest possible contact force, as each ball traverses the defect area. In addition, the balls in the loaded region carry the highest share of load, resulting in elevated contact forces.

To analyze the envelope spectrum, a bandpass filter was applied to the time-domain signal to isolate fault-induced impacts. The filtered signal was then processed using the Hilbert transform.

Figure 5 shows the envelope spectra of a ball bearing with an outer race defect positioned at various angles (0°, 90°, 180°, and 270°). As observed in the spectra, there is periodic excitation of the bearing system as the balls traverse the defective area. The presence of lower frequency components, such as Fundamental Train Frequency (FTF), reflects modulation by the balls and cage dynamics. Furthermore, the shaft frequency (F_s) component is also present. This is because the defect impacts are modulated by the rolling element kinematics, which are synchronized to the shaft rotation. At all

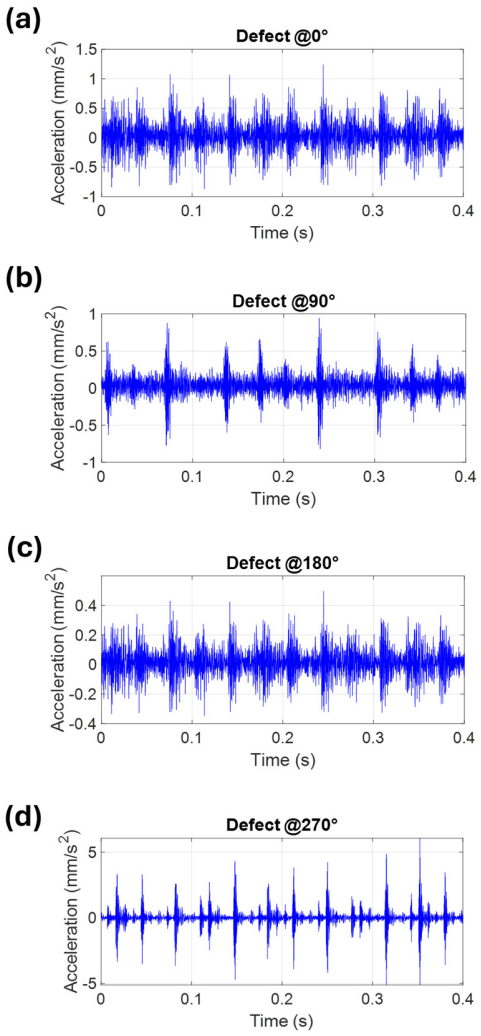

Fig. 4. Vertical Time-domain response of a bearing with an outer defect at 0°, 90°, 180°, and 270°.

positions, the dominant component is the BPFO at approximately 107 Hz, along with its higher harmonics at 2 × BPFO, 3 × BPFO. In Figure 5(b), the amplitude of BPFO at 90° is illustrated as ±0.18, while Figures 5(a) and 5(c) show the/an amplitude of ±0.2. The presence of BPFO harmonics in the envelope spectrum is consistent with the findings in [18], where similar results were reported from both the numerical and experimental analyses. This confirms the periodic impulsive excitation generated as each rolling element passes the defect zone. The amplitudes of BPFO and its harmonics are distinguishable from the noise floor. The highest amplitude occurs at 270°, as exhibited in Figure 5(d), where the defect is positioned directly beneath the load region. This is attributed to the increased contact forces in this region. The results showed that the severity of impacts decreases as the defect is positioned further from the maximum load zone.

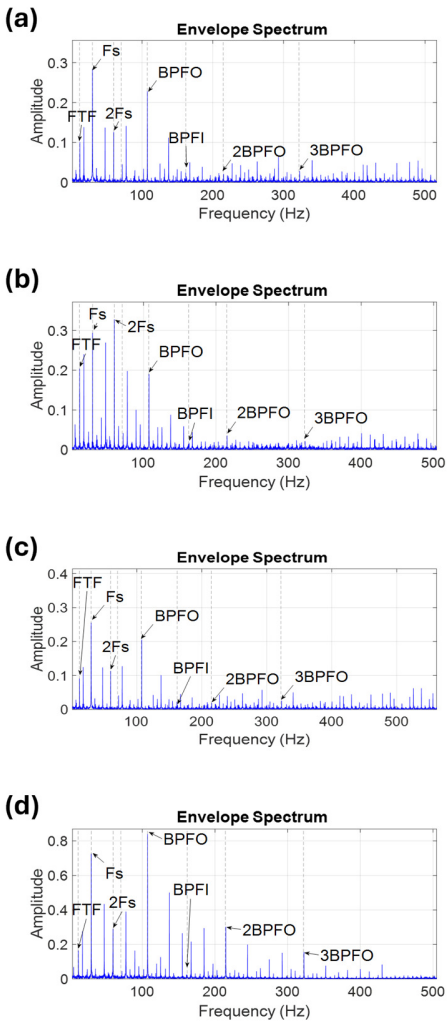

Fig. 5. Envelope spectra of a bearing with an outer race defect at (a) 0°, (b) 90°, (c) 180°, and (d) 270°.

VII. CONCLUSIONS

This study demonstrated that the angular position of an outer race spall defect strongly governs the vibration response. Defects located at 270°, within the maximum load zone, produced the highest amplitudes, while positions at 0°, 90°, and 180° generated weaker signals due to reduced contact forces. The envelope analysis consistently revealed modulation at the Ball Pass Frequency of the Outer Race (BPFO) and its harmonics, highlighting their diagnostic significance. The results confirmed that defect orientation directly influences the detectability of faults and must be incorporated into monitoring strategies to improve accuracy.

Future work should focus on validating the model under variable speeds and load conditions, while also extending it through experimental analysis to better capture nonlinear behavior, lubrication effects, and scenarios with multiple defects. Furthermore, the application of advanced signal processing techniques is proposed to enhance the diagnostic accuracy and support the development of intelligent maintenance frameworks.

ACKNOWLEDGMENT

The authors express sincere gratitude to the Vaal University of Technology, Department of Industrial Engineering, Operations Management, and Mechanical Engineering, and the NRF for providing support for the successful completion of this research.

REFERENCES

[1] O. Rathodkar and P. Jain, "Analysis of Effects of Increase in Defect Size on Vibration of a Ball Bearing," *International Journal of Mechanical Engineering*, vol. 9, pp. 1–11, Oct. 2022, https://doi.org/10.14445/23488360/IJME-V9I10P101.

[2] C. Malla and I. Panigrahi, "Review of Condition Monitoring of Rolling Element Bearing Using Vibration Analysis and Other Techniques," *Journal of Vibration Engineering & Technologies*, vol. 7, pp. 407–414, 2019, https://doi.org/10.1007/s42417-019-00119-y.

[3] T. Mashiyane, D. Desai, and L. Tartibu, "Numerical simulation of the effect of angular misalignment on the dynamic behaviour of bearing," *in Proceedings of the MATEC Web of Conferences*, Stellenbosch, South Africa, 2022, vol. 370, https://doi.org/10.1051/matecconf/202237009003.

[4] F. Combet and X. Thomas, "Modelling and diagnosis of a crack of a bearing inner ring," France.

[5] Y. Bella, A. Oulmane, and M. Mostefai, "Industrial Bearing Fault Detection Using Time-Frequency Analysis," *Engineering, Technology & Applied Science Research*, vol. 8, no. 4, pp. 3294–3299, Aug. 2018, https://doi.org/10.48084/etasr.2135.

[6] L. Liang, C. Liu, and F. Liu, "Bearing fault diagnosis based on singular value distribution of impulse response segment," *ISA Transactions*, vol. 134, pp. 511–528, Mar. 2023, https://doi.org/10.1016/j.isatra.2022.08.015.

[7] M. Wang, K. Yan, X. Zhang, and J. Hong, "Research on the Dynamic Properties of Ball Bearings Based on the Quasi-Static Method," *Advances in Mechanical Design*, vol. 111, pp. 281–290, 2022, https://doi.org/10.1007/978-981-16-7381-8_19.

[8] S. Chen, D. Zou, X. Chen, Y. Wang, and D. Cai, "Support Force and Load Distribution Analysis of Angular Contact Ball Bearing Considering Rotor Deformation," *Tribology Online*, vol. 18, no. 4, pp. 125–135, 2023, https://doi.org/10.2474/trol.18.125.

[9] J. Liu, L. Xue, L. Wang, Z. Shi, and M. Xia, "A new impact model for vibration features of a defective ball bearing," *ISA Transactions*, vol. 142, pp. 465–477, Nov. 2023, https://doi.org/10.1016/j.isatra.2023.08.014.

[10] D. Ruan, C. Gühmann, and J. Yan, "A new solving method for ball bearing dynamics model based on optimization with nonlinear constraints: Contact angles as iterative variables," *Journal of Manufacturing Processes*, vol. 106, pp. 338–346, Nov. 2023, https://doi.org/10.1016/j.jmapro.2023.09.076.

[11] Y. Wu, C. Zhang, J. Wang, and S. Xu, "Dynamic Modeling of Rolling Bearing Outer Ring Failure with Time-Varying Excitation Under Contact Deformation," *in Proceedings of the UNIfied Conference of DAMAS, IncoME and TEPEN Conferences (UNIfied 2023)*, Huddersfield, United Kingdom, 2023, pp. 777–783, https://doi.org/10.1007/978-3-031-49413-0_59.

[12] K. More et al., "Vibrational analysis of faulty deep-groove ball bearing under radial load," *Frontiers in Mechanical Engineering*, vol. 11, Apr. 2025, https://doi.org/10.3389/fmech.2025.1560986.

[13] A. Rashed, A. G. E.-M. Ahmed, and M. Ali, "CONDITION MONITORING OF LOCALIZED OUTER RACE DEFECTS OF TAPER ROLLER BEARINGS USING VIBRATION ANALYSIS," *Journal of the Egyptian Society of Tribology*, vol. 20, no. 1, pp. 51–62, Jan. 2023, https://doi.org/10.21608/jest.2023.284023.

[14] F. Wang, X. Ling, Z. Zhang, P. Dai, S. Yan, and L. Wang, "The Effect of Fit Clearance between Outer Race and Housing on Vibration Characteristics of a Cylindrical Roller Bearing with Localized Defects," *Machines*, vol. 10, no. 6, 2022, Art. No. 415, https://doi.org/10.3390/machines10060415.

[15] A. Nabhan, M. Nouby, A. Sami, and M. Mousa, "Vibration analysis of deep groove ball bearing with outer race defect using ABAQUS," *Journal of Low Frequency Noise, Vibration and Active Control*, vol. 35, no. 4, pp. 312–325, 2016, https://doi.org/10.1177/0263092316676414.

[16] Y. Tian, C. Yan, W. Luo, Y. Liu, and L. Wu, "Dynamic Modeling and Stability Analysis of High-Speed Angular Contact Ball Bearing," *in Proceedings of TEPEN 2022*, Baotou, China, 2022, pp. 818–828, https://doi.org/10.1007/978-3-031-26193-0_72.

[17] C. Zhang, Y. Wu, S. Xu, F. Qin, L. Wu, and B. Ouyang, "Dynamic modeling and analysis of rolling bearing faults under time-varying excitations considering defect deformation," *Journal of Vibroengineering*, vol. 26, no. 4, pp. 776–792, 2024, https://doi.org/10.21595/jve.2024.23672.

[18] A. H. A. Mattar, H. Sayed, Y. K. Younes, and H. H. El-Mongy, "Experimental Verification and Nonlinear Dynamic Response Analysis of a Rolling Element Bearing with Localized Defects," *Journal of Failure Analysis and Prevention*, vol. 22, pp. 1753–1770, 2022, https://doi.org/10.1007/s11668-022-01466-x.